Trans Indian Inst Met (2025) 78:274
https://doi.org/10.1007/s12666-025-03744-2

ORIGINAL ARTICLE

Thermodynamic and Experimental Study of Roasting and Leaching of Low-Grade Molybdenum Concentrates for Industrial Calcium Molybdate Production

Tatyana Oleinikova[1] · Lyutsiya Karimova[1] · Tansholpan Tussupbekova[1] · Irina Terentyeva[1] · Bolotpay Baimbetov[1] · Guldana Makasheva[1]

Received: 15 July 2025 / Accepted: 22 October 2025
© The Indian Institute of Metals - IIM 2025

Abstract
Purpose The study addresses the development of an environmentally sustainable and economically efficient technology for processing low-grade molybdenum ore. Methodology: Particular attention was given to the effect of roasting temperature on the phase composition of intermediate products and the subsequent recovery of molybdenum. Experiments were carried out in 2023 using ore from a Kazakhstan molybdenum deposit. Results: The results showed that roasting at 550 °C provided the most favorable conditions, yielding up to 88.28% molybdenum trioxide (MoO_3) and ensuring a high extraction rate of molybdenum into solution (97.79%). From the purified solution, calcium molybdate ($CaMoO_4$) was obtained that complied with MDK-2 grade requirements, with molybdenum content of 47.6%, phosphorus 0.0317%, and sulfur 0.253%. These findings demonstrate that even low-quality ores can be efficiently processed to produce a commercially valuable product, while minimizing both material losses and environmental impact.

Keywords Calcium molybdate · Extraction · Leaching · Molybdenum by-product · Roasting

1 Introduction

Molybdenum is a rare metal widely used in metallurgy, the chemical industry, and other sectors due to its unique properties, such as high melting point and corrosion resistance [1]. In 2023, global molybdenum production reached approximately 300,000 tons, with China leading at about 37% of the total, followed by the USA and Chile. These three countries together account for nearly 85–90% of global production [2, 3]. Kazakhstan ranks fourth worldwide, possessing estimated reserves of 1.1 million tons across around 20 deposits, many of which remain underutilized due to challenges in ore beneficiation and the production of high-quality concentrates. Some deposits are currently exploited as sources of copper or tungsten, with molybdenum recovered as a by-product [1].

The primary raw materials for producing ferromolybdenum and other molybdenum compounds are molybdenum concentrates and industrial by-products [4]. Beneficiation is commonly performed using flotation, which efficiently separates molybdenite from gangue minerals, while gravity concentration and magnetic separation are applied less frequently. Copper–molybdenum ores are typically processed using collective flotation schemes to obtain combined concentrates, which are further refined using sodium sulfide and thermal treatment in closed circuits to minimize harmful emissions [5]. Tungsten–molybdenum ores and molybdenum–uranium ores are processed using gravity flotation or hydrometallurgical methods, depending on the ore composition and the desired products [5–8].

Rising demand from the steel, oil, and gas industries for corrosion-resistant alloys, cast iron, and catalysts has gradually depleted high-quality molybdenum ore reserves [5]. Consequently, there is increasing interest in processing low-grade ores efficiently, minimizing losses, and maximizing economic return [9–12]. Various processing methods exist, each with advantages and limitations. Pyrometallurgical methods rely on oxidative roasting of molybdenite (MoS_2) to produce molybdenum trioxide (MoO_3), suitable for further production of ferromolybdenum,

✉ Lyutsiya Karimova
lyutsiya_karimova@alibagl.com

[1] LLP KazHydroMed, Moskovskaya Str. 4, Karaganda 100000, Republic of Kazakhstan

Published online: 27 November 2025

though associated with molybdenum and rhenium losses and requiring gas and dust treatment [11]. Pyro-hydrometallurgical methods combine roasting with leaching, sorption, and extraction, achieving high molybdenum recovery and enabling rhenium separation but requiring precise chemical control [10]. Combined methods use sintering with additives such as sodium sulfate and carbon to convert molybdenum into water-soluble forms, effective for low-quality raw materials but dependent on ore composition [9]. Bio-hydrometallurgical approaches employ microorganisms to oxidize molybdenum sulfides, offering environmentally safe processing for poor ores, albeit with longer processing times [13].

The pyro-hydrometallurgical process remains the industry standard for molybdenum production, encompassing roasting, leaching, purification, and electrolysis. Roasting is critical for impurity removal, increasing molybdenum concentration, and enhancing material reactivity [13–18]. Oxidation during roasting occurs at temperatures above 500 °C, forming calcine (molybdenum oxide), which is further processed to produce pure MoO_3 [19]. Key reactions include:

$$CuS + 1.5O_2 \rightarrow CuO + SO_2$$

$$2FeS_2 + 5.5O_2 \rightarrow Fe_2O_3 + 4SO_2$$

$$As_2S_3 + 5.5O_2 \rightarrow As_2O_5 + 3SO_2$$

In the presence of metal oxides, sulfurous gases oxidize to SO_3 and react to form sulfates:

$$CuO + SO_3 \rightarrow CuSO_4$$

$$Fe_2O_3 + 3SO_3 \rightarrow Fe_2(SO_4)_3$$

Sulfides of Cu, Fe, Zn, and Pb convert into oxides and sulfates, and at 500–700 °C, molybdates are formed:

$$MeO + MoO_3 \rightarrow MeMoO_4$$

$$MeSO_4 + MoO_3 \rightarrow MeMoO_4 + SO_3$$

$$MeCO_3 + MoO_3 \rightarrow MeMoO_4 + CO_2$$

Given the depletion of high-grade molybdenum ores and increasing industrial demand, developing technologies for processing low-quality molybdenum by-products is essential. Conventional methods often fail to maximize molybdenum yield while ensuring environmental safety, highlighting the need for efficient, economically viable, and sustainable processing approaches.

The study aims to develop and optimize an environmentally sustainable technology for processing low-quality molybdenum ore to obtain commercial calcium molybdate with high yield and minimal losses.

The study investigated the impact of roasting temperature on the phase composition of molybdenum by-products, as well as the conversion of molybdenum into soluble forms. Additionally, the study focused on optimizing roasting and leaching conditions to maximize molybdenum extraction. A technological scheme for producing calcium molybdate was developed and the quality of the end product evaluated. Finally, the practical significance of the proposed technology in processing low-quality raw materials was evaluated.

The developed approach enables processing of low-grade molybdenum ore with high economic and environmental efficiency, achieving up to 97.8% molybdenum extraction and producing commercial calcium molybdate meeting MDK-2 grade standards (47.6% Mo). This technology is suitable for enterprises working with poor ores and secondary molybdenum products, particularly relevant amid limited high-quality resources.

2 Methods and Materials

The molybdenum by-product used in this study was obtained in 2023 from copper–molybdenum ore sourced from the Republic of Kazakhstan. Its chemical composition was first determined using traditional silicate chemical analysis, while gold and silver contents were measured by fire assay. Major and trace elemental concentrations were confirmed using Inductively Coupled Plasma Mass Spectrometry (ICP-MS) (Table 1).

The mineralogical composition of the by-product was examined using a combination of optical microscopy and X-ray diffraction (XRD). Thin polished sections were studied in reflected light using an OLYMPUS BX 53 optical

Table 1 Chemical composition of molybdenum by-product

Components	Composition, %	Components	Composition, %
Mo	22.23	As	0.0180
Cu	7.516	Co	0.0278
Au, g/t	10.6	P	0.12
Ag, g/t	167.0	Cd	< error
Fe	16.54	Re, g/t	62.3
Zn	0.049	Bi	< error
Pb	0.053	Ni	0.0143
Al/Al_2O_3	1.126/2.128	Ca/CaO	1.155/1.617
Si/SiO_2	5.33/11.422	C	9.57
Mg/MgO	0.741/1.230	S_{total}	27.85
Sb	0.000635	$S_{sulfide}$	27.60
U	0.0304	$S_{sulfate}$	0.256
Ba	< error	F	< error

microscope to identify individual ore minerals and evaluate their liberation and association. The distribution of molybdenite and associated sulfides is shown in Fig. 1.

Molybdenite was the predominant mineral, typically occurring in flake-like, tabular, or scaly forms, with 80% present as liberated grains (0.003–0.5 mm). The remaining molybdenite was mostly associated with chalcopyrite or other sulfides (Fig. 2). Chalcopyrite was present mainly in a free state (grain size 0.003–0.06 mm) and occasionally intergrown with molybdenite or other minerals, as illustrated in Fig. 3.

The mineral composition of the by-product in Figs. 2 and 3 was determined using X-ray diffraction (XRD) analysis, complemented by X-ray fluorescence (XRF) for elemental verification. The XRD patterns were matched with reference standards from the ICDD database to identify crystalline phases, while XRF provided quantitative support for the elemental composition.

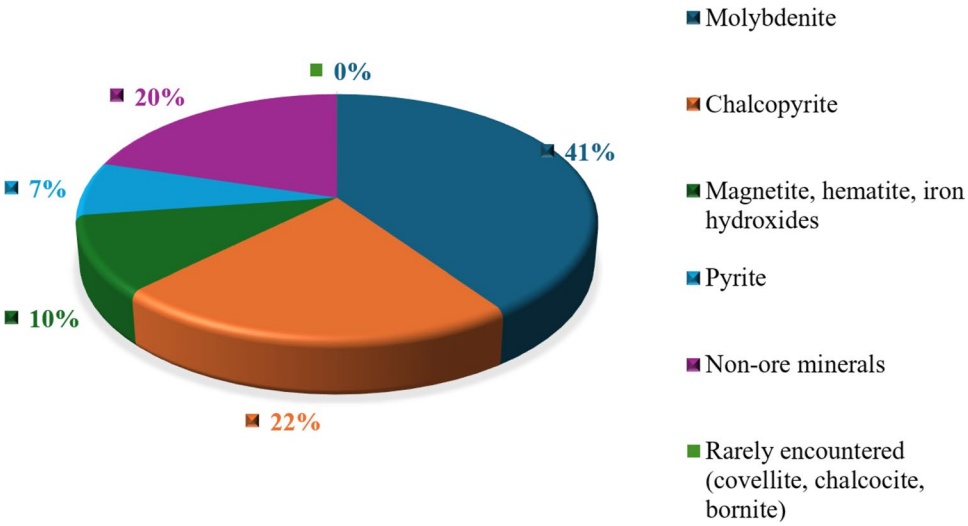


Fig. 1 Ore mineralization of Mo by-product

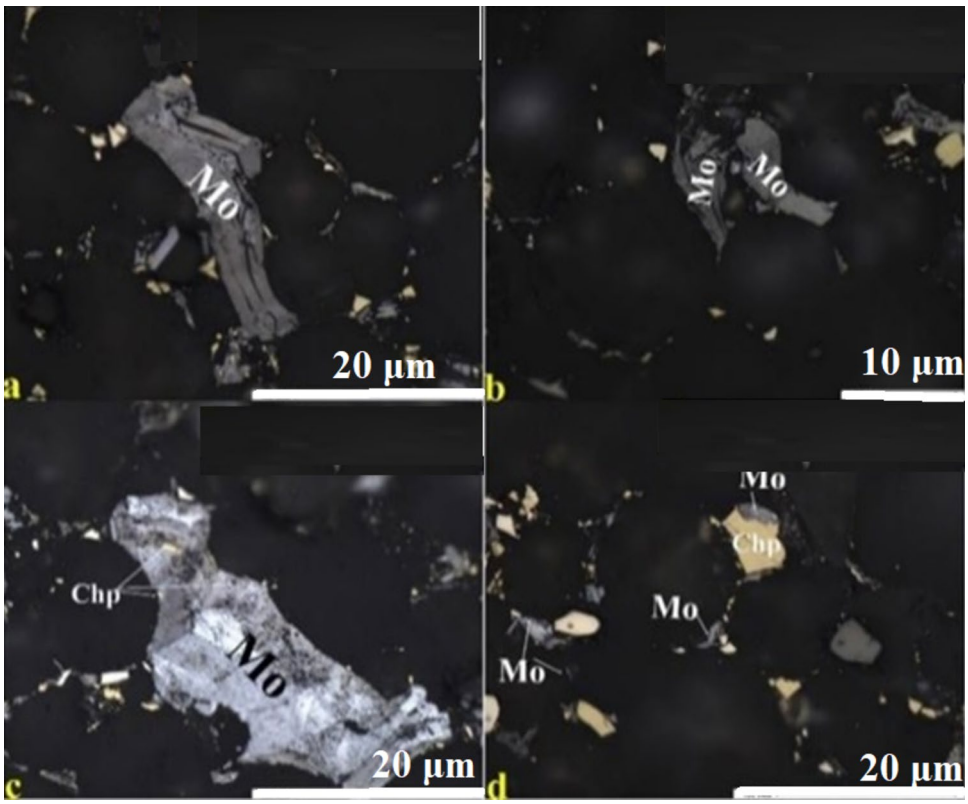


Fig. 2 Characteristics of molybdenite forms and aggregates. Magnified 20/10. Note: Chp—chalcopyrite, Mo—molybdenite; A and B—magnification of 20 µm and 10 µm for inclusions of molybdenum; C and D—magnification of 20 µm for inclusions of intergrown molybdenum and chalcopyrite and single inclusions of molybdenum. Source: Karimova [20]

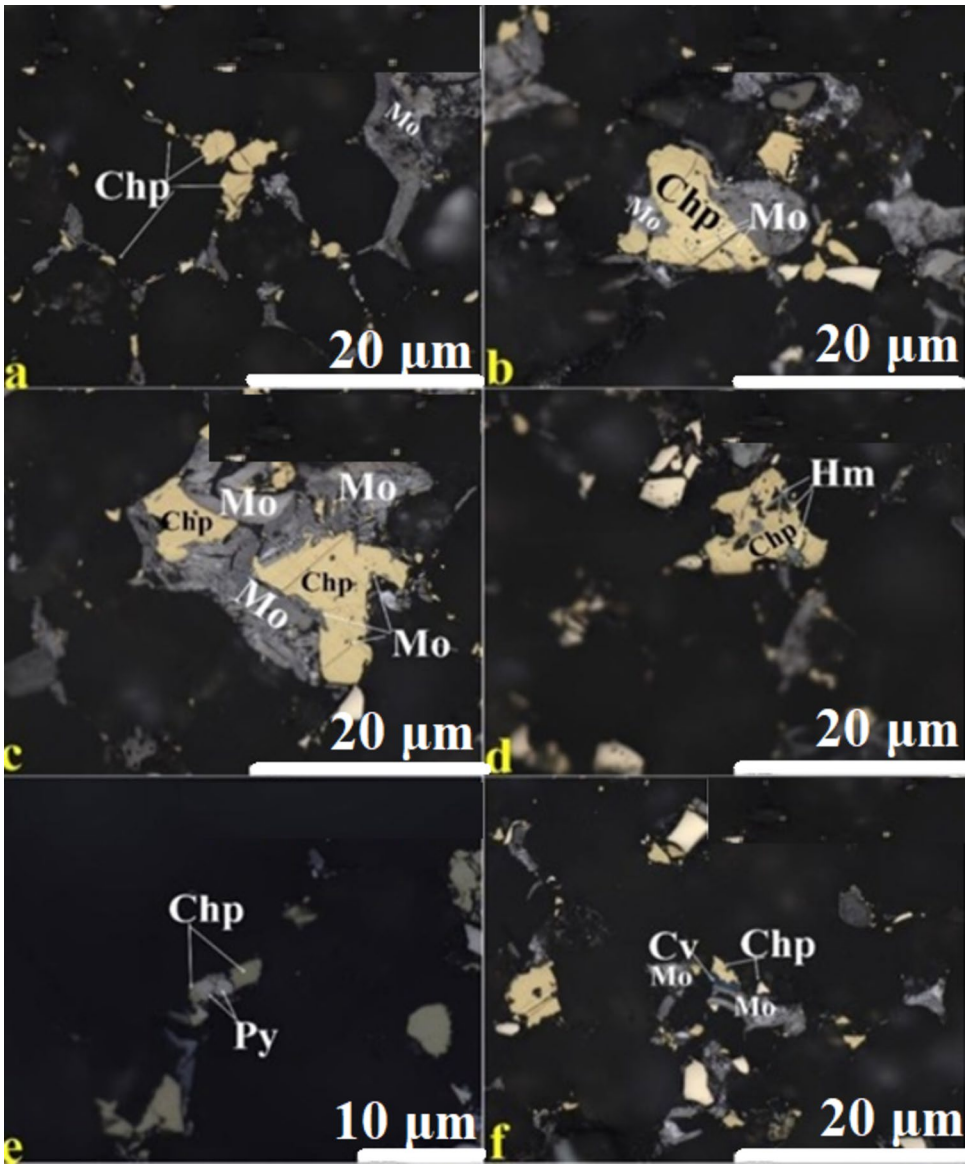


Fig. 3 Characteristics of chalcopyrite precipitates. Magnified 500/1000. Note: Chp—chalcopyrite, Mo—molybdenite, Hm—hematite, Py—pyrite, Cv—covellite. a—non-fusion of chalcopyrite and molybdenum at 20 μm; b—fusion of molybdenum and chalcopyrite at 20 μm; c—massive fusion of chalcopyrite and molybdenum, 20 μm; d—fusion of chalcopyrite and hematite at 20 magnification, e—fusion of chalcopyrite and pyrite at 10 μm, f—fusion of covellite, molybdenum, and chalcopyrite at 20 μm

The XRD analysis was carried out using a Bruker D2 Phaser diffractometer with Cu Kα radiation, operating at 30 kV and 10 mA, with a scanning step of 0.02° 2θ and a counting time of 1 s per step. Phase identification was performed by matching the experimental diffraction patterns with the ICDD database. The main phases detected were MoS_2 (molybdenite), $CuFeS_2$ (chalcopyrite), Fe_2O_3 (hematite), and MoO_3, with the corresponding peaks assigned to specific 2θ values (Fig. 4).

Oxidative roasting experiments were performed in a muffle furnace (SNOL 15/1200). Calcine was produced by roasting the molybdenum by-product at temperatures ranging from 300 °C to 700 °C for 2 h under atmospheric conditions. The temperature was continuously monitored using a DEPK 145–0919.1000.1 thermocouple.

The key reactions considered included oxidation of molybdenite to molybdenum trioxide:

$$2MoS_2 + 7O_2 \rightarrow 2MoO_3 + 4SO_2$$

and formation of iron molybdate:

$$Fe_2O_3 + MoO_3 \rightarrow 2FeMoO_4$$

Thermodynamic feasibility of these reactions was evaluated via Gibbs free energy (ΔG) calculations as a function of temperature. Results indicated that MoS_2 oxidation is spontaneous above 400 °C, while $FeMoO_4$ formation is favored between 500 and 600 °C. XRD patterns of the calcine at various temperatures were recorded to monitor phase transformations.

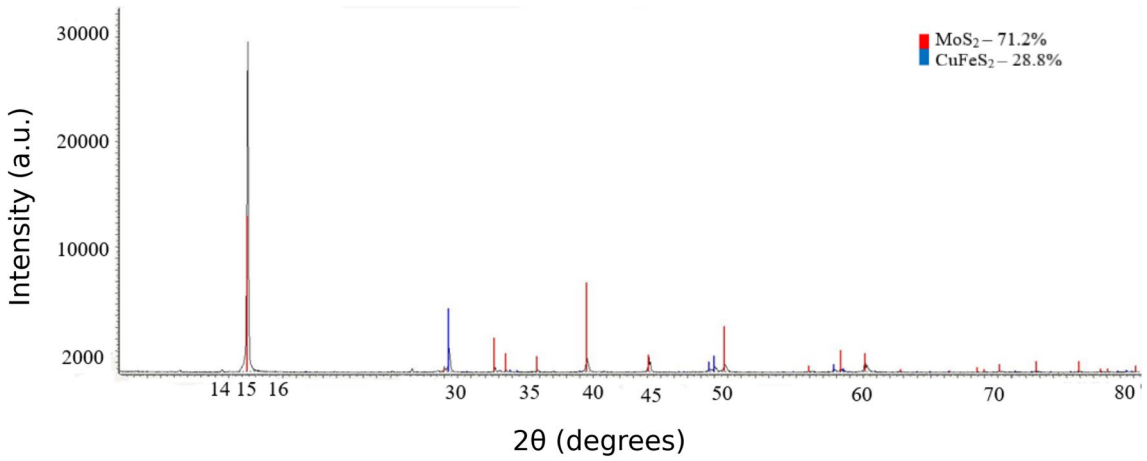


Fig. 4 X-ray phase composition of molybdenum by-product

Leaching experiments were conducted in a thermostated reactor with mechanical stirring to ensure uniform mixing. The process was conducted at a temperature of 90 °C, using a liquid-to-solid ratio of 10:1. Leaching took place for 120 min using a 10% sodium carbonate (Na_2CO_3) solution as the leaching agent.

After leaching, the solution was filtered to remove residues, then heated to 80–90 °C, and neutralized to pH 7.3. Calcium chloride (500 g/L) was added dropwise to precipitate calcium molybdate ($CaMoO_4$). The precipitate was boiled for 60 min, washed with distilled water to reduce residual sulfates, filtered, dried, and calcined. The overall process is summarized in Fig. 5, including roasting, leaching, solution purification, and precipitation stages.

The leachate was analyzed for Mo, Cu, and Fe content using ICP-MS to determine extraction efficiency. XRD

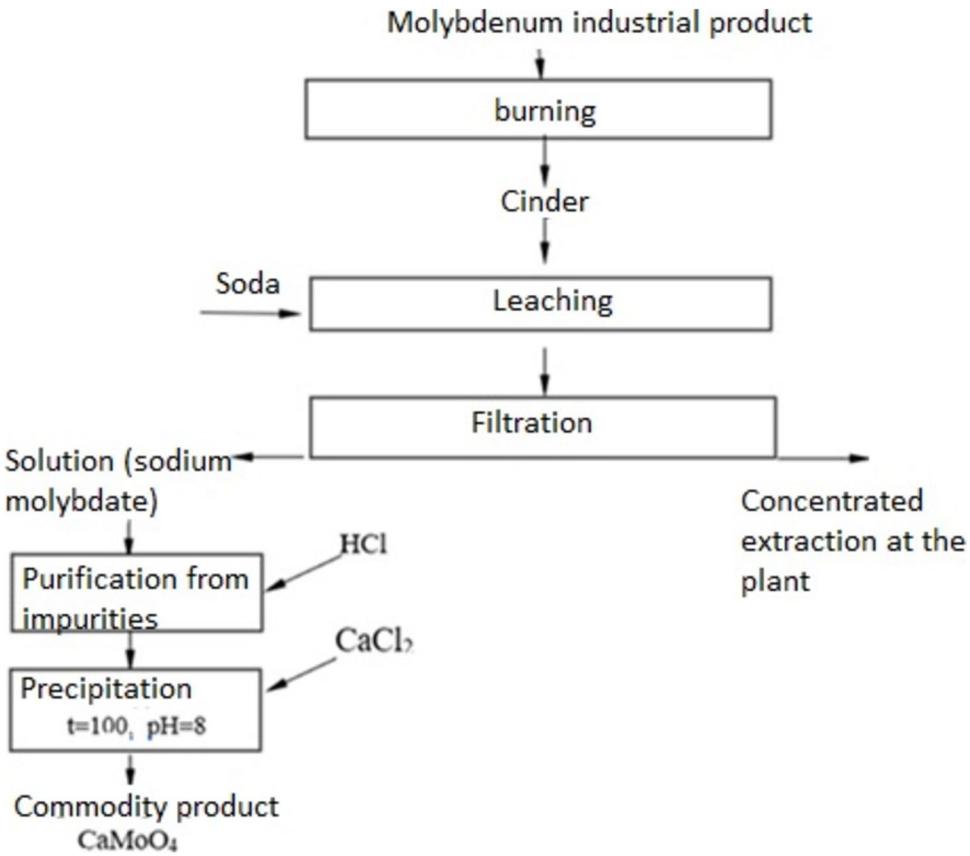


Fig. 5 Conceptual technological scheme for obtaining calcium molybdate from molybdenum by-product using oxidative roasting

patterns were employed to identify the main phases after roasting and leaching, and the results were compared with thermodynamic predictions to verify consistency between experimental observations and expected reaction pathways.

In addition to the procedures described above, several steps were taken to ensure the reliability and reproducibility of the experiments. All roasting and leaching experiments were performed in triplicate. Temperature and pH were continuously monitored and recorded to control the experimental conditions precisely. The particle size distribution of the by-product before and after roasting was measured using laser diffraction. Specific surface area and porosity of calcines were determined via BET analysis to assess changes in mineral accessibility.

Furthermore, the thermodynamic calculations included Gibbs free energy, enthalpy, and equilibrium constants over the temperature range of interest. Pourbaix diagrams were constructed to visualize the stability regions of molybdenum, iron, and sulfur species under different pH and potential conditions, aiding in the interpretation of leaching behavior. All experimental data were statistically processed using standard deviation and mean values, and comparisons between treatments were carried out to evaluate the effect of temperature and leaching parameters on extraction efficiency.

Finally, the experimental results were integrated with phase identification and thermodynamic predictions to provide a comprehensive understanding of the roasting and leaching process. This approach allows for correlation between observed mineral transformations, phase evolution, and leaching efficiency, ensuring that both practical and theoretical aspects of the process are addressed.

3 Results

Calcines were obtained by oxidative roasting of molybdenum by-product in the temperature range of 350–700 °C. The chemical composition of the calcines is summarized in Table 2, showing clear trends in the redistribution of elements with increasing roasting temperature.

The data reveal several consistent trends. Calcine yield decreases progressively with increasing temperature, indicating the intensification of the decomposition of the original mineral matrix. Molybdenum content remains relatively stable within the range of 21.96–22.11%, demonstrating its resistance to volatilization under the applied roasting conditions. By contrast, the contents of copper and iron decline at temperatures above 400 °C, reflecting their partial oxidation and the formation of soluble species. Sulfur content decreases sharply beyond 400 °C due to the release of SO_2 accompanying MoS_2 oxidation. Rhenium content increases with temperature, suggesting that it is liberated from the molybdenite lattice during oxidation. Meanwhile, calcium content gradually decreases, likely due to the formation of calcium sulfates or other secondary phases.

The chemical reactions occurring during roasting were examined with thermodynamic calculations using ΔG vs. T plots (Figs. 6, 7).

As shown in Fig. 7, the oxidation of MoS_2 and $CuFeS_2$ becomes thermodynamically favorable above 400 °C, while the stabilization of $Fe_2(MoO_4)_3$ is predicted in the range of 500–600 °C. These results are consistent with the observed decrease in sulfur content (Table 2) and the increase in refractory Fe-containing phases.

$$2MoS_2 + 7O_2 \rightarrow 2MoO_3 + 4SO_2,\ \Delta G < 0 \text{ for } T > 400°C$$

Similarly, formation of iron molybdate ($Fe_2(MoO_4)_3$) occurs optimally between 500 and 600 °C, in agreement with the increased $Fe_2(MoO_4)_3$ content observed in XRD analysis.

Diffractometric analysis of the calcines shows significant changes in phase composition with increasing roasting temperature. At 350–400 °C, molybdenite (MoS_2) dominates, accompanied by quartz and chlorite. As the temperature rises to 500–550 °C, molybdenite gradually oxidizes to molybdite (MoO_3), while iron molybdate ($Fe_2(MoO_4)_3$) and powellite ($CaMoO_4$) begin to form, reaching maximal concentrations around 550 °C. Hematite (Fe_2O_3) and chabazite also increase with temperature, reflecting oxidation and stabilization of iron- and aluminum-containing minerals. Calcite decomposes above 400 °C. At 700 °C, new phases such as copper–iron molybdate ($CuFe(MoO_4)_3$), sodalite, and albite appear, indicating high-temperature phase transformations. Overall, the

Table 2 Chemical composition of calcines at different roasting temperatures

Temperature, °C	Yield, %	Mo, %	Cu, %	S, %	Fe, %	Zn, %	Re, g/t	Ca, %
350	100.0	22.11	7.615	26.73	16.514	0.049	70.59	1.237
400	99.33	21.99	8.00	13.83	17.412	0.052	61.96	1.287
500	94.67	21.96	8.295	4.05	17.126	0.055	39.99	1.396
550	91.67	22.00	8.41	3.51	17.96	0.055	33.98	1.302
600	89.67	21.96	8.247	1.25	17.854	0.060	18.86	1.376
700	82.67	22.00	8.99	0.68	20.30	0.066	2.59	1.465

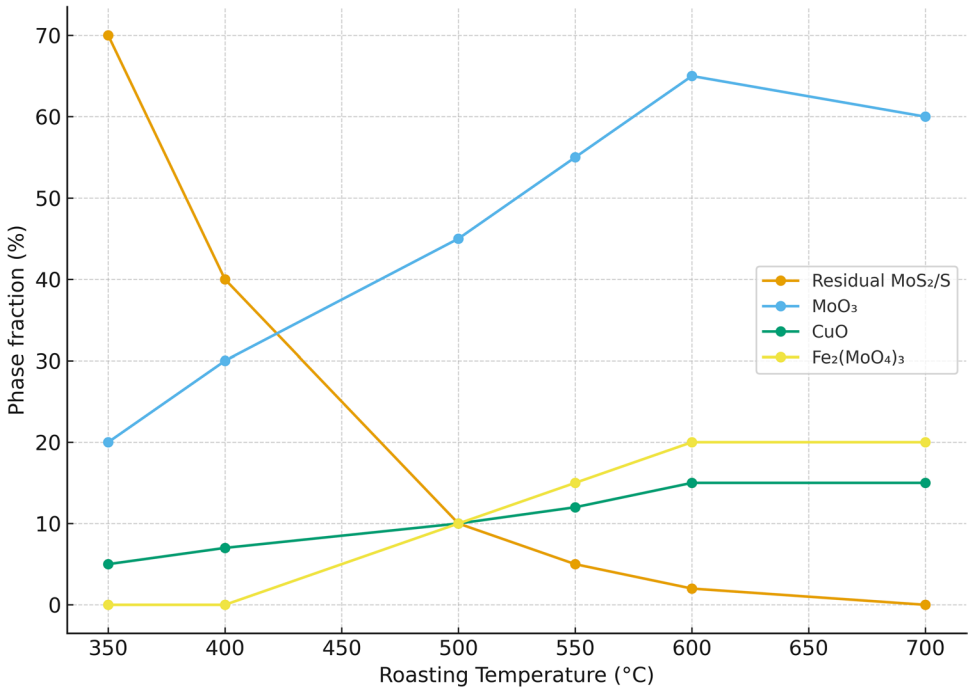


Fig. 6 Cumulative evolution of phases during roasting

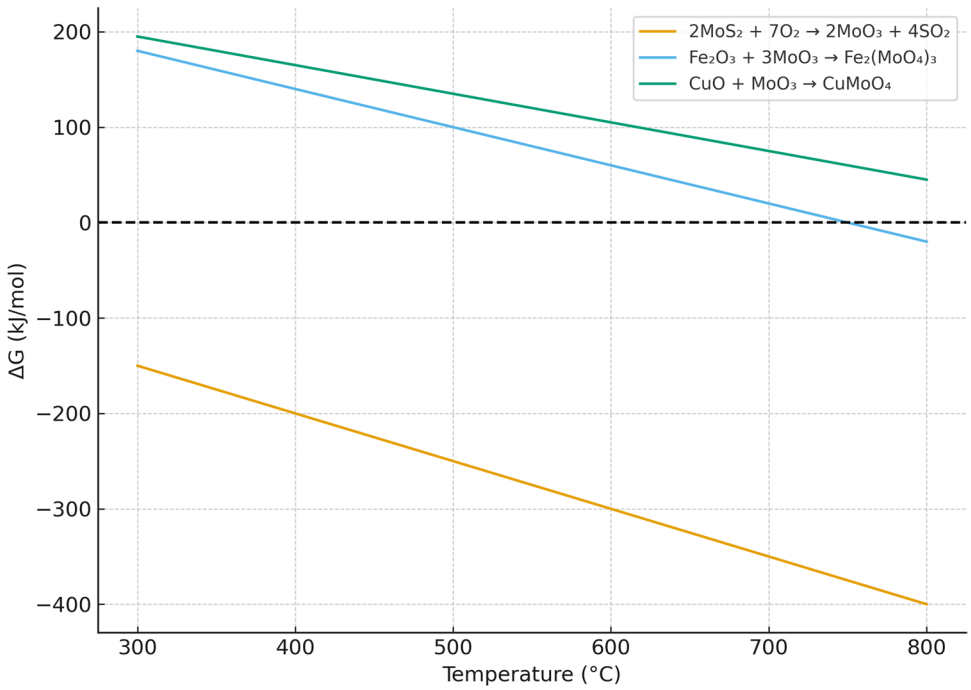


Fig. 7 Thermodynamic feasibility of main reactions during oxidative roasting (ΔG vs. T)

data indicate that higher roasting temperatures promote the conversion of molybdenum and iron into more stable, extractable mineral forms.

Calcines roasted at 350–700 °C were subjected to aqueous leaching with sulfuric acid under controlled conditions (T = 25 °C, pulp density 10%, L/S = 5:1, 2 h). The metal recovery was calculated using:

$$\text{Recovery}\ (\%) = (C_{leach} \cdot V / C_{calcine} \cdot m) \cdot 100$$

where C_{leach} is the concentration of metal in the leachate, V the leachate volume, $C_{calcine}$ the initial metal concentration in the calcine, and m the mass of calcine.

Figure 8 illustrates the change in the phase composition of the calcine depending on the roasting temperature. The

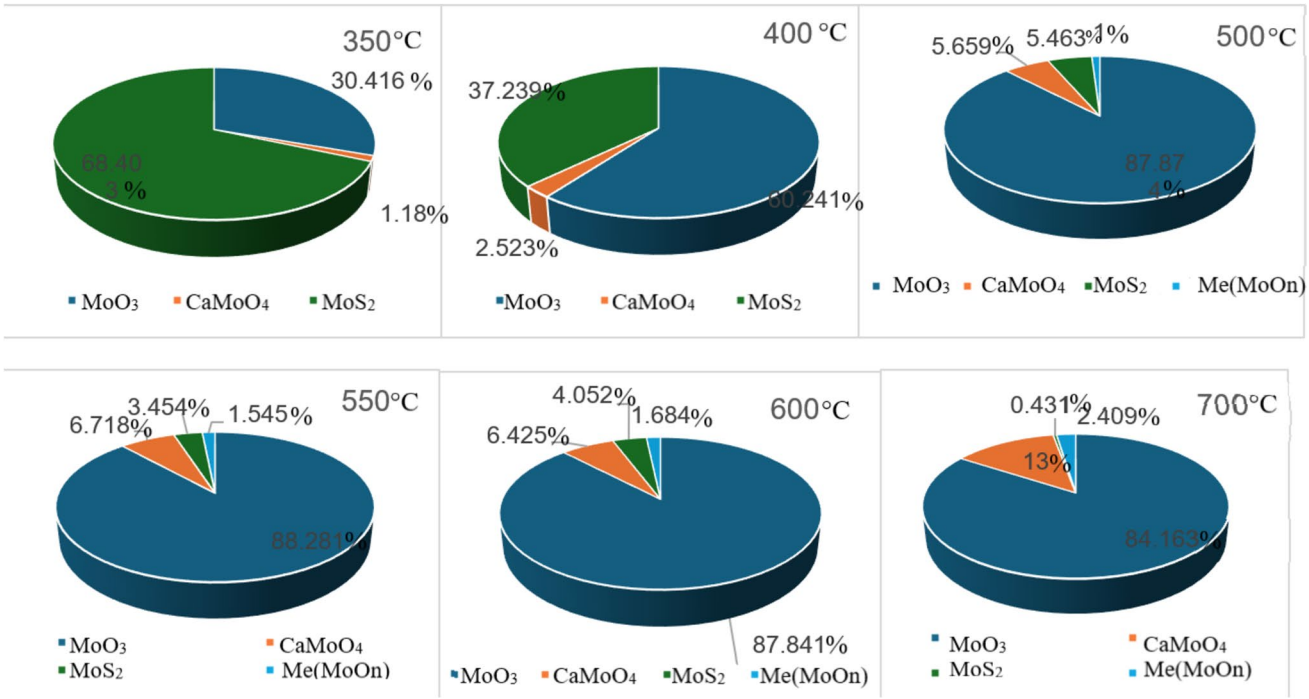


Fig. 8 Change in the phase composition of calcine depending on roasting temperature

highest content of oxidized molybdenum forms is observed at 550 °C.

Table 3 presents the recovery of Mo, Cu, Fe, and Re.

Table 3 shows that molybdenum recovery increases steadily with roasting temperature and reaches a maximum at 600 °C, while copper recovery also improves consistently across the temperature range. In contrast, iron recovery decreases sharply with increasing temperature, and rhenium recovery shows a pronounced decline above 500 °C. These trends indicate that higher roasting temperatures favor selective enrichment of Mo and Cu, but reduce the retention of Re and Fe.

The recovery of molybdenum steadily increased with roasting temperature up to 600 °C, reflecting the enhanced formation of soluble molybdenum trioxide (MoO_3). Similarly, copper recovery increased with temperature due to the transformation of chalcopyrite ($CuFeS_2$) into more leachable oxides, such as CuO. However, iron recovery decreased significantly, which is consistent with the formation of insoluble iron molybdates ($Fe_2(MoO_4)_3$) and hematite (Fe_2O_3). Rhenium recovery was maximized at temperatures between 350 and 400 °C, but declined at higher temperatures, likely due to partial volatilization or incorporation into refractory phases.

X-ray diffraction (XRD) analysis of calcines roasted at different temperatures revealed distinct phase evolution. At 350–400 °C, the dominant phase was MoS_2, with minor amounts of $CuFeS_2$ and traces of elemental sulfur present. Between 500 and 550 °C, MoS_2 was largely oxidized to MoO_3, while $CuFeS_2$ transformed into CuO and Fe_2O_3, accompanied by the initial formation of $Fe_2(MoO_4)_3$. At 600–700 °C, the predominant phases were MoO_3, $Fe_2(MoO_4)_3$, and minor CuO, with residual sulfur falling below detection limits.

Table 3 Recovery of Mo, Cu, Fe, and Re at different roasting temperatures

Roasting Temp, °C	Mo Recovery, %	Cu Recovery, %	Fe Recovery, %	Re Recovery, %
350	85.2	42.7	15.3	78.6
400	88.1	46.5	12.8	76.4
500	91.3	52.9	8.2	68.5
550	92.5	55.7	5.9	63.2
600	93.1	57.4	3.1	49.8
700	92.8	59.9	1.2	25.7

Figure 9 illustrates the evolution of crystalline phases with roasting temperature. At 350 °C, strong MoS_2 reflections dominate, while above 500 °C, MoO_3 and $Fe_2(MoO_4)_3$ peaks intensify, reaching a maximum at 550–600 °C. At 700 °C, the diffraction patterns indicate stabilization of refractory iron molybdates and minor CuO phases.

Key XRD peaks (2θ values) and corresponding phases are summarized in Table 4.

X-ray diffraction (XRD) analysis was performed on calcines obtained after oxidative roasting of molybdenum by-products at 350, 450, 550, 600, and 700 °C. The diffraction patterns confirmed the progressive transformation of molybdenite (MoS_2) into molybdenum trioxide (MoO_3), with minor formation of iron molybdate ($Fe_2(MoO_4)_3$) and traces of Cu-containing phases.

At 350 °C, the diffraction patterns revealed dominant MoS_2 peaks at 2θ angles of approximately 14.4°, 33.0°, 39.5°, 49.7°, and 58.9°, suggesting that the material was not fully oxidized. Minor MoO_3 peaks appeared at $2\theta \approx 23.3°$ and 25.7°, reflecting the initial formation of oxide phases. Increasing the temperature to 450 °C caused the intensity of the MoS_2 peaks to decrease, while the intensity of the MoO_3 peaks increased at $2\theta \approx 23.3°$, 25.7°, 26.3°, 27.3°, 34.4°, and 39.4°. Small $Fe_2(MoO_4)_3$ reflections were also detected at 2θ ≈ 31.1°, 36.9°, and 48.1°, indicating the onset of refractory, Fe-containing phase formation.

At 550 °C, the MoS_2 peaks were almost undetectable and the MoO_3 peaks dominated the pattern (2θ ≈ 23.3°, 25.7°, 26.3°, 27.3°, 34.4°, and 39.4°). The $Fe_2(MoO_4)_3$ reflections intensified at 2θ ≈ 31.1°, 36.9°, and 48.1°, consistent with the increasing precipitation of refractory iron phases.

Table 4 XRD peaks of calcine phases at different 2θ angles

2θ (°)	Phase	Intensity
23.3	MoO_3	Strong
28.6	CuO	Medium
33.5	Fe_2O_3	Medium
37.8	$Fe_2(MoO_4)_3$	Weak → Strong with T
50.0	MoO_3	Medium

Further heating to 600 °C maintained strong MoO_3 peaks, while the $Fe_2(MoO_4)_3$ peaks persisted at 2θ ≈ 31.1°, 36.9°, and 48.1°, indicating the stabilization of the iron molybdate phase. Minor CuO peaks also appeared at 2θ ≈ 35.5° and 38.7°. At 700 °C, there was a slight decrease in the intensity of the MoO_3 peaks at 2θ ≈ 23.3°, 25.7°, and 26.3°, whereas the $Fe_2(MoO_4)_3$ reflections remained stable. This suggests that less soluble phases were forming under leaching conditions.

Overall, the XRD results confirm that roasting at 550–600 °C optimizes the formation of leachable MoO_3 while minimizing residual MoS_2 and undesirable phases such as MoO_2. The evolution of peak intensities across temperatures aligns with the observed extraction efficiency during subsequent leaching.

ΔG calculations indicate that oxidation of MoS_2 to MoO_3 and $CuFeS_2$ to $CuO + Fe_2O_3$ is favorable above 400 °C, consistent with XRD observations. The formation of $Fe_2(MoO_4)_3$ is favored at 500–600 °C, as shown by $\Delta G < 0$ in this range. Pourbaix diagrams for Mo and Cu in acidic

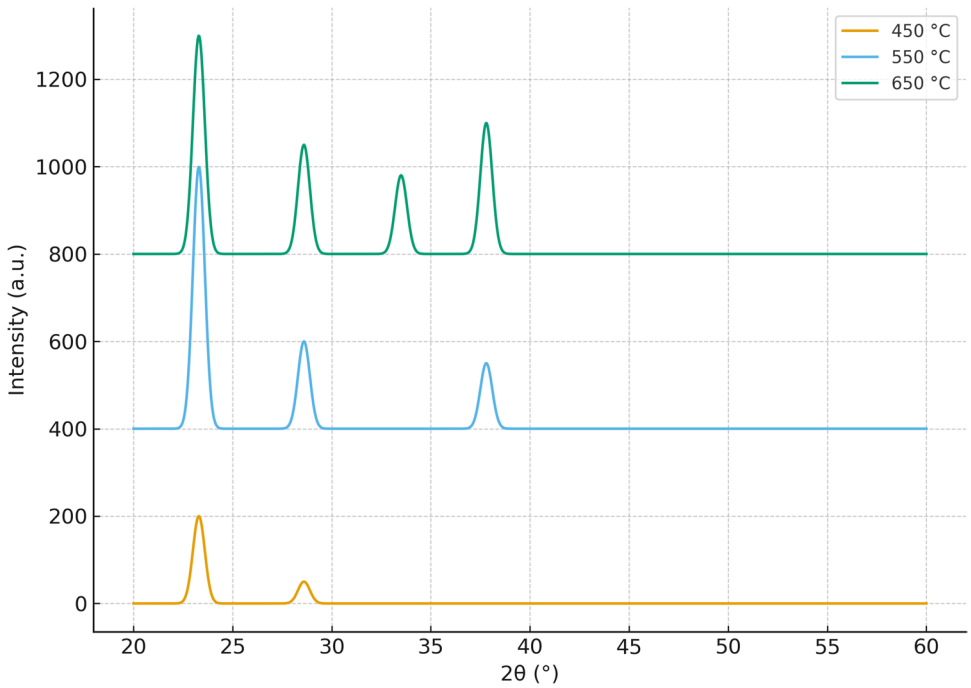


Fig. 9 XRD patterns of calcines roasted at different temperatures (350–700 °C)

conditions explain the selective leaching behavior: MoO_3 is soluble in H_2SO_4 (pH < 2), CuO dissolves partially, while $Fe_2(MoO_4)_3$ and Fe_2O_3 remain insoluble.

Figure 7 (cumulative phase plot) summarizes the relative abundance of phases as a function of roasting temperature. The MoO_3 fraction increases from around 20% at 350 °C to 65% at 600 °C, while the CuO fraction rises from 5 to 15% within the same temperature range. $Fe_2(MoO_4)_3$ begins to form above 500 °C, reaching approximately 20% at 600 °C. Residual MoS_2 and elemental sulfur are almost completely absent by 600 °C, indicating near-complete oxidation of the original sulfide phases.

This cumulative diagram demonstrates the progressive oxidation of sulfides and formation of leachable oxides and refractory phases, correlating directly with observed metal recovery trends.

4 Discussion

The roasting of molybdenum by-products is fundamentally governed by thermodynamic principles. Oxidative conversion of MoS_2 to MoO_3 becomes spontaneous above 400 °C, as indicated by negative Gibbs free energy ($\Delta G < 0$), which aligns with the observed phase transformations in XRD patterns. Formation of iron molybdate ($Fe_2(MoO_4)_3$) is favored between 500 and 600 °C, consistent with the maximum precipitation of refractory Fe-containing phases and the observed decrease in Fe recovery during leaching. Careful control of roasting temperature is therefore essential to maximize the formation of soluble MoO_3 while minimizing undesirable phases such as MoO_2 that can reduce extraction efficiency. Overall, temperatures around 550–600 °C optimize molybdenum conversion into leachable forms and ensure the stability of the calcine for subsequent processing.

Leaching efficiency is closely related to the chemical stability of the roasted phases. MoO_3 is highly soluble under acidic conditions, while $Fe_2(MoO_4)_3$ and Fe_2O_3 remain largely insoluble. This explains the selective recovery observed experimentally: Molybdenum achieves high extraction (up to 97%), copper is partially recovered due to CuO formation, and iron remains predominantly in refractory molybdate or oxide forms. Controlling solution pH and redox conditions during leaching prevents unwanted dissolution or precipitation reactions and justifies the use of sodium carbonate under controlled conditions for calcium molybdate precipitation.

Integrating thermodynamic reasoning with experimental observations provides a clear understanding of roasting and leaching processes. The selected roasting temperature range ensures the formation of leachable MoO_3 and $CaMoO_4$, minimizes losses, and reduces environmental impact, offering a thermodynamically sound basis for the efficient recovery of molybdenum from low-grade by-products.

This study investigated the roasting of molybdenum concentrate at various temperatures to optimize the processing of low-grade molybdenum ore for the production of commercial calcium molybdate. It was found that increasing the roasting temperature leads to a decrease in calcine yield, reflecting molybdenite decomposition and redistribution of components, while molybdenum content in the calcine remains stable. At the same time, copper, sulfur, and iron decrease, likely due to their partial dissolution or formation of less stable phases.

X-ray diffractometry confirmed that higher roasting temperatures promote gradual oxidation of molybdenite to MoO_3 and iron molybdate, facilitating subsequent molybdenum extraction. Leaching tests demonstrated that molybdenum extraction increases significantly between 500 and 600 °C, exceeding 96%. The optimal roasting temperature for maximal molybdenum recovery was identified as 550 °C, in agreement with literature data [21–23]. Using soda for calcine leaching achieved molybdenum extraction up to 97.79%.

Overall, an efficient technology was developed for processing molybdenum by-products, producing calcium molybdate with high molybdenum yield and minimal losses of other elements. Comparison with the literature confirmed the general trends observed during roasting. At low temperatures (300–500 °C), molybdenite is only partially oxidized, forming intermediate phases such as Mo_2S_3, consistent with our observations at 350–400 °C [24]. At medium temperatures (550–600 °C), MoO_3 becomes dominant in the calcine, aligning with previous reports [25], and maximal molybdenum extraction is achieved. High-temperature roasting (650–700 °C) leads to near-complete oxidation to MoO_3 [26], while temperatures above 700 °C may cause partial dissociation and formation of metallic molybdenum or other phases [27]. Literature suggests that the optimal temperature range for pure MoO_3 formation and calcine stabilization is 550–650 °C [28–32], which is consistent with our findings. Calcines also contained molybdates, sulfates, silica, aluminosilicates, and other compounds [33, 34].

Some *limitations* should be noted. Only one type of molybdenum concentrate was studied, and the temperature range was limited to 350–700 °C. Further studies, including higher temperatures, different concentrates, and industrial-scale tests, are needed to confirm and expand the applicability of these results. Long-term stability assessments under operational conditions were not conducted but are important for practical applications in metallurgy and chemical industries.

Nevertheless, this research significantly contributes to developing technology for processing low-quality molybdenum ore. It identifies optimal oxidative roasting temperatures

ensuring maximal molybdenum extraction with minimal losses and provides a detailed evaluation of calcine composition and leaching efficiency. The roasting temperature range of 550–600 °C proved most effective for producing calcium molybdate with high molybdenum content (up to 47.6%), meeting industrial standards, and enabling high-yield processing of low-grade raw materials.

5 Conclusions

This study developed an environmentally sustainable method of processing molybdenum by-products into high-purity calcium molybdate. Optimized roasting at 550–600 °C achieved over 97% molybdenum extraction and stable formation of $CaMoO_4$ with a molybdenum content of 47.6%. The process uses safe reagents, such as sodium carbonate, and remains efficient when processing various low-grade feedstocks. This approach offers a practical route for sustainable molybdenum recovery by combining high yield, environmental safety, and industrial feasibility. Future work will focus on process scaling and product purification.

Acknowledgements Not applicable.

Author contributions *Tatyana Oleinikova helped in* conceptualization, formal analysis, writing—review and editing; *Lyutsiya Karimova contributed to* project administration, resources, writing—original draft; *Tansholpan Tussupbekova helped in* funding acquisition, supervision, writing—original draft; *Irina Terentyeva was involved in* visualization, writing—original draft, validation; *Bolotpay Baimbetov helped in* data curation, investigation, writing—review and editing; *Guldana Makasheva contributed to* software, methodology, writing—review and editing.

Funding The research received no funding.

Data availability All data generated or analyzed during this study are included in this published article.

Declarations

Conflict of interests The research has no conflict of interest.

References

1. Semoto Y, Suyantara G P W, Miki H, Sasaki K, Hirajima T, Tanaka Y, Aoki Y, and Ura K, *Minerals.* **11** (2021) 1377. https://doi.org/10.3390/min11121377
2. Castro S, Lopez-Valdivieso A, and Laskowski J S, *Int J Miner Process* **148** (2016) 48–58. https://doi.org/10.1016/j.minpro.2016.01.003
3. Yi G, Macha E, Van Dyke J, Macha R E, McKay T, and Free M L, *Miner Eng.* **295** (2021) 102466. https://doi.org/10.1016/j.cis.2021.102466
4. Shi L, Wang X W, Wang M Y, Peng J, and Xiao C, *Hydrometallurgy* **108** (2011) 214–219. https://doi.org/10.1016/j.hydromet.2011.04.009
5. Lianyong W, Wenqiang S, Jingfan Z, and Jiuju C, *Rare Met Mater Eng* **44** (2015) 2618–2622. https://doi.org/10.1016/S1875-5372(16)60005-X
6. Fan X H, Qiong D, Min G, and Chen X L, *Trans Nonferrous Met Soc China* **29** (2019) 840–848. https://doi.org/10.1016/S1003-6326(19)64994-0
7. Guiqing Z, Separation of molybdenum and vanadium, in Kuangdi X (ed) *The ECPH Encyclopedia of Mining and Metallurgy,* Springer (2024), pp 1901–1902. https://doi.org/10.1007/978-981-99-2086-0_775
8. Wang L, Guo P, Pang J, Luo L, and Zhao P, *Vacuum* **116** (2015) 77–81. https://doi.org/10.1016/j.vacuum.2015.03.006
9. Han G, Feng Y, You M, Sun H, Su S, Liu B, and Huang Y, *Cleaner Eng Technol.* **22** (2024) 100809. https://doi.org/10.1016/j.clet.2024.100809
10. Liu Q, Liu R, Yang S, Feng W, and Wang M, *Minerals* **13** (2022) 35. https://doi.org/10.3390/min13010035
11. Liu R, Zhao Z, and Li Y, *Sep Purif Technol* **322** (2023) 124269. https://doi.org/10.1016/j.seppur.2023.124269
12. Zhang F, Liu C, Chandrasekar S, Li Y, and Xu F, *Int J Miner Metall Mater* **31** (2024) 91–105. https://doi.org/10.1007/s12613-023-2727-1
13. Gao B, Jiang H, Zeng M, Peng M, Hu L, Zhang W, and Mao L, *J Cleaner Prod.* **367** (2022) 132976. https://doi.org/10.1016/j.jclepro.2022.132976
14. Cheema H A, Bhatti I A, Srivastava R R, Jahan N, and Zia M A, *Chem Pap* **76** (2022) 4049–4058. https://doi.org/10.1007/s11696-022-02145-9
15. Ilhan S, *Can Metall Q* **59** (2020) 26–35. https://doi.org/10.1080/00084433.2020.1715691
16. Karacahan M K, *J Sustain Metall* **9** (2023) 1564–1577. https://doi.org/10.1007/s40831-023-00748-4
17. Liu B, Zhang B, Han G, Wang M, Huang Y, Su S, Xue Y, and Wang Y, *Resour Conserv Recycl.* **181** (2022) 106232. https://doi.org/10.1016/j.resconrec.2022.106232
18. Liu X, Zou J, Zhao Z, Chen X, Li J, He L, and Sun F, *J Environ Chem Eng.* **12** (2024) 114833. https://doi.org/10.1016/j.jece.2024.114833
19. Aleksandrov P V, Medvedev A S, Imideev V A, Berbenev A O, and Kochurov K I, *Metallurgist* **64** (2021) 940–948. https://doi.org/10.1007/s11015-021-01075-3
20. Karimova L, Kairalapov Y, Tussupbekova T, Oleinikova T and Makasheva G, *J Min Metall, Sect B Metall* 60 (2024) 71–83. https://aseestant.ceon.rs/index.php/jmm/article/view/45674
21. Cai Y, Ma L, Xi X, and Nie Z, *J Clean Prod.* **380** (2022) 135018. https://doi.org/10.1016/j.jclepro.2022.135018
22. Khalife H, and Rezaei M, *Miner Eng* **209** (2024) 108614. https://doi.org/10.1016/j.mineng.2024.108614
23. Zhang Q, Liu T, Zhang Y, Xue N, and Zheng Q, *Sep Purif Technol* **279** (2021) 119578. https://doi.org/10.1016/j.seppur.2021.119578
24. Baba AA, Adeyemi CO and Mohapatra M, *Preparation of high-grade sodium molybdate-dihydrate from a low-grade moly ore as corrosion resistant,* 2023 SSRN 4374476.
25. Zhang J, Xue N, Zhang Y, and Zheng Q, *Processes* **11** (2023) 470. https://doi.org/10.3390/pr11020470
26. Yang S, Liu Y, Wang M, Liu S, He S, and Zhao Y, *JOM* **76** (2024) 2491–2500. https://doi.org/10.1007/s11837-024-06396-7
27. Zeng L, Wang M, Xiao C, Wu S X, Guan W J, Qing-gang L I, and Cao Z Y, *Trans Nonferrous Met Soc China.* **32** (2022) 1314–1324. https://doi.org/10.1016/S1003-6326(22)65876-X
28. Zykova A V, Krivoshchekov S V, Isakov D A, Guryev A M, and Belousov M V, *Drug Dev Reg.* **13** (2024) 164–170. https://doi.org/10.33380/2305-2066-2024-13-2-1724
29. Bogomolov NG, Ostrikova TO, Tranova YuS, Fomicheva DA … & Chernykh IV, *Herbarium* 2 (2025) 30–36. https://doi.org/10.33380/3034-3925-2025-2-3-43

30. Shestak V A, and Tsyplakova A D, *Ugol* **10** (2022) 72–76. https://doi.org/10.18796/0041-5790-2022-10-00-00
31. Aleshin D S, Krasheninin A G, Tanutrov I N, and Reutov D S, *Metallurgist* **67** (2023) 879–885. https://doi.org/10.1007/s11015-023-01574-5
32. Liang X, Tang J, Li L, Wu Y, and Sun Y, *J Clean Prod* **376** (2022) 134108. https://doi.org/10.1016/j.jclepro.2022.134108
33. Arkhipov V P, Kuzina N A, and Filippov A, *Appl Magn Reson* **52** (2021) 607–617. https://doi.org/10.1007/s00723-021-01323-4
34. Yu H, Liu C, Liu S, Gu Y, Wang S, Yaraş A, Hu L, Zhang W, Peng M, Arslanoğlu H, and Mao L, *J Hazard Mater.* **464** (2024) 132982. https://doi.org/10.1016/j.jhazmat.2023.132982

Publisher's Note Springer Nature remains neutral with regard to jurisdictional claims in published maps and institutional affiliations.

Springer Nature or its licensor (e.g. a society or other partner) holds exclusive rights to this article under a publishing agreement with the author(s) or other rightsholder(s); author self-archiving of the accepted manuscript version of this article is solely governed by the terms of such publishing agreement and applicable law.